BEST: Journal of Recent Trends in General Engineering & Research (BEST: JRTGER)
Vol. 2, Issue 1, June 2017, 49-60

PROCESSING MAP FOR HOT WORKING CHARACTERISTICS OF A 2205 CAST DUPLEX STAINLESS STEEL

M. POUYAMANESH[1], V. JAVAHERI[2], H. RASTEGARI[3], GH. R. EBRAHIMI[4] & B. EGHBALI[5]

[1]Department of Materials Engineering, Esfarayen University, Esfarayen, Iran

[2]Department of Material Engineering and Production Technology, University of Oulu, Oulu, Finland

[3]Department of Mechanical and Materials Engineering, Birjand University of Technology, Birjand, Iran

[4]Department of Materials Engineering, Hakim Sabzevari University, Sabzevar, Iran

[5]School of Materials Engineering, Sahand University of Technology, Tabriz, Iran

ABSTRACT

In the present study, the constitutive flow behavior of a 2205 cast duplex stainless steel has been evaluated during warm compression testing in the temperature range 900-1100 °C at strain rates in the range 0.001-0.1 s^{-1}, aided with the micro structural characterization of deformed specimens. Moreover, the constitutive analysis of flow stress was carried out using the hyperbolic sine function, and the material constants were determined. In this context, various deformation mechanisms, including dynamic re crystallization, occurring during warm deformation have been characterized and delineated through construction of a processing map by establishing a power dissipation map and an instability map for the steel and superimposing them. The result shows dynamic re crystallization occurred in the range 900-1030 °C and 0.001-0.003 s^{-1} with a power dissipation efficiency of 50-60%. In the instability regime, various micro structural defects such as flow localization, kinking and cavities appeared. In this regard, the deformation activation energy of the steel was estimated to be ~263 KJ/Mol.

KEYWORDS: Hot Deformation, Flow Behavior, Processing Map, Constitutive Relationship, Cast 2205 Duplex Stainless Steel

INTRODUCTION

Duplex stainless steels (DSSs) are a special class of steels owing to the duplex microstructure. In this regard, DSSs have higher strength than austenitic stainless steels, higher toughness than ferritic stainless steels, good weld ability, and high resistance to stress corrosion cracking [1-2]. It is well known that the good properties of duplex stainless steels rely on a two-phase microstructure comprising approximately equal amounts of austenite and ferrite [3-4]. Due to their unique combination of corrosion and mechanical properties, DSSs are widely used in many industrial applications [5-6]. As a member in the family of the DSSs, 2205 steel is the most popular material for chemical engineering and oil refining, power plants, food, pharmaceutical, and marine industries, as well as many other fields [7-8].

DSSs can be processed by different routes, i.e. casting, forging, extrusion or rolling. These forming operations are usually performed at high temperature, at least in their first stages. The hot deformation of DSSs is notoriously more complex than those of ferritic or austenitic stainless steels because of different thermal expansion coefficients and deformation characteristics of austenite and ferrite which may easily cause the formation of defects in the microstructure during hot deformation [9-10].

It is established that ferrite (crystal lattice: BCC), with rather high stacking fault energy, easily undergoes dynamic recovery (DRV) to soften during hot deformation. On the other hand, austenite (crystal lattice: FCC), characterized by significantly lower stacking fault energy, undergoes only limited dynamic recovery and is likely to have dynamic re crystallization (DRX) [5]. Hence, the variation in flow stress of the DSSs during hot deformation is rather complex, because it is influenced by various interconnected metallurgical phenomena such as work hardening, DRV and DRX [11].

To evaluate the hot deformation characteristics of the DSSs, it was considered appropriate to construct a processing map based on the principles of the dynamic material model (DMM) developed by Prasad et al. [12, 13] in order to optimize the workability and controlling the microstructure of the product and to avoid 'unsafe' domains and/ or instability regime/s in processing.

Recently, many researchers have been using this technique to evaluate the hot deformation characteristics of a wide range of metallic materials [7] but there is still a lack of knowledge related to the study on hot working characteristics of 2205 DSSs using processing maps. In the present study, an attempt has been made in order to identify the optimum deformation conditions of a cast 2205 DSS for achieving the desired micro structure using a processing map method.

EXPERIMENTAL PROCEDURE

The material used in this study was an as-cast slab of 2205 DSS, which was annealed at 1250°C for 2 hours. Chemical composition of the DSS is given in Table 1. Cylindrical specimens of (8 mm x 10 mm were machined for hot compression tests parallel to the solidification direction.

Table 1: Chemical Compositions of Samples.

C	Si	Mn	S	P	Ni	Cr	Mo	Nb	Cu	Fe
0.07	0.40	0.67	0.01	0.01	6.40	20.76	2.90	0.06	0.38	Balanced

Figure 1: shows an optical micrograph of a representative initial microstructure consisting of secular austenite distributed in the ferrite matrix. The starting microstructure of the studied material consisted of about 40% ferrite (dark region) and a 60 % estimate (light region). Hot compression tests were conducted on Z250 Zwick/Roe uniaxial thermo-mechanical simulator equipped with a resistance furnace.

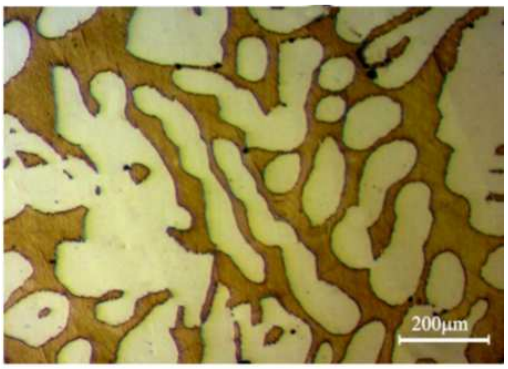

Figure 1: The Initial Microstructure of 2205 Duplex Stainless Steel Used in this Study

The specimens were preheated to 1200 °C, held for 8 min and then cooled to the deformation temperature at the rate of 10°Cs−1. All specimens were held at the deformation temperature for 10s to eliminate thermal gradients prior to deformation. Hot compression tests were performed in the temperature of 900, 1000 and 1100 °C and constant engineering

strain rates of 0.001, 0.01 and 0.1 s^{-1}. It also should be noted that, all samples were compressed in a single hit to a true strain of 0.7, and immediately quenched in order to study the micro structural evolutions under high temperatures.

In order to minimize friction, and hence barreling effect, graphite lubricant was employed between the specimen surface and the anvils. A thermocouple was spot welded to the longitudinal center of the specimen to control the temperature. For metallographies examination, deformed specimens were sectioned at mid-plane parallel to the compression axis. After Grinding, polishing and etching (HCl and potassium meta Bi sulphite, K2S2O5 were used as agent), microstructures were characterized in the central location of each specimen using an Olympus GX51 optical microscopy.

RESULT AND DISCUSSION

Flow Stress

Stress correction due to frictional effects was performed according to Ebrahimi and Najafizadeh method [14], and then smoothing the flow curve with a sixth to ninth-order polynomial was applied. Smoothed true stress-strain curves obtained for different temperatures and strain rates are summarized in Figure 2.

As obvious, the flow behavior of the austenite + ferrite microstructure was affected by deformation temperature and strain rate. The flow stress tends to increase with decreasing temperature and increasing strain rate. In addition, the higher strain rate at a given temperature leads to an increase in peak stress. At a strain rate of 0.001 s^{-1} and 0.01 s^{-1}, the flow curves exhibit flow softening after a peak followed by the onset of a steady-state at the specified string. As known, the onset of dynamic re crystallization during compression, due to the softening effect, might be identified by a distinct peak in the stress-strain curve (strain hardening effect) followed by flow softening [15, 16]. It can be noted that when the true strain is smaller than 0.03, the true stress increases rapidly with the increase of true strain owing to the dominant effect of work hardening. By increasing the true strain larger than 0.03, the rate of work hardening decreases due to occurrence of the DRV. With deformation going on, the softening effect is more significant than hardening due to occurrence of DRX. Hence, true stress decreases after reaching a peak value, and then keeps a steady state as softening and hardening effects are basically in balance. It can be clearly seen that the steady state region can be easily achieved at the high deformation temperature and low strain rate. Indeed, the higher temperature can cause higher mobility to the grain boundaries and the lower strain rate can provide longer time for the dislocation annihilation, nucleation and growth of DRX [17]. The flow curves at 0.1 s^{-1} and the temperature 1000 and 1100°C are of steady state type, no flow softening occurred in these conditions. There is no obvious peak stress in these curves, as dynamic re crystallization never or rarely occurs in the deformation process. Ebrahimi et al. [18] believed that continual formation and dissolution of low angle boundaries and to a constant density of unbound or free dislocations within the sub grains is the main reason of this trend.

Figure 4 shows the effect of strain rate on peak stress at different temperatures. As shown in the figure, the peak stress increases with increase of strain rate at the same temperature, while it decreases with increase of temperature at the same strain rate (as expected), which indicates that the 2205 steel is very sensitive to the deformation temperature and strain rate.

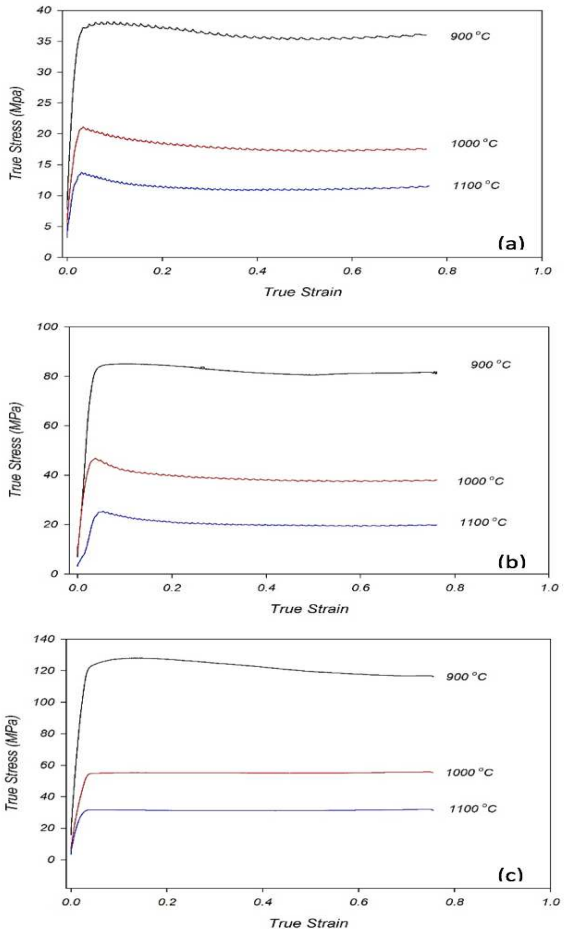

Figure 2: True Stress–Strain Curves of 2205 Duplex Stainless Steel under Hot Compression at Different Strain Rate Of: (A) 0.001 S^{-1}; (B) 0.01 S^{-1}; And(C) 0.1 S^{-1}

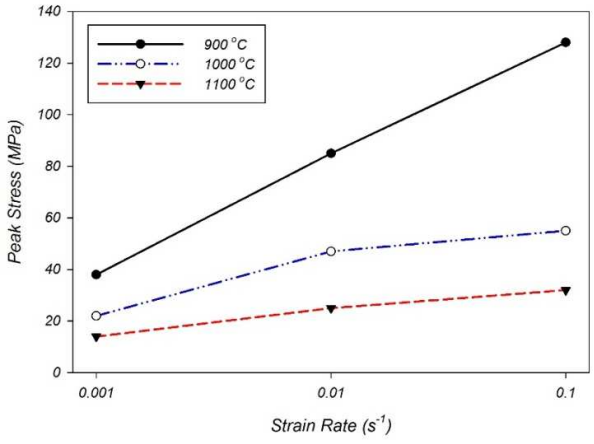

Figure 3: Effect of Strain Rate on Peak Stress at Different Temperatures

Calculation of Activation Energy and Z Parameter

In the literatures, the most widely applied technique for modeling of flow stress of a material during deformation is the equation which correlates the Zener– Hollomon parameter (Z) to the flow stress (σ):

$$Z = \varepsilon^{o} \exp(Q/RT) = f(\sigma) \quad \text{Equation 1}$$

Where Z is temperature compensated strain rate, εo is the strain rate, Q is the activation energy of deformation, R is the universal gas constant (equal to 8.314 J/Mol K) and T is the deformation temperature the Z parameter can be related to the flow stress in different ways including power law description, exponential law description and hyperbolic sine law description. Among these, the hyperbolic sine law ones (Eq. (2)) Covers a wide range of temperatures and strain rates for hot deformation modeling.

After taking logarithms, it can be written as:

$$Z = \dot{\varepsilon} \exp(Q/RT) = A[\sinh(\alpha\sigma)]^{n} \quad \text{Equation 2}$$

where A, n and α are known as apparent material constants. In this equation, peak stress was selected for determination of flow stress. In this regard, by taking the logarithm from Eq. (2), the following expression (Eq. 3) could be derived for peak stress:

$$\ln \dot{\varepsilon} + Q/R\,(1/T) = \ln A + n \ln\{\sinh(\alpha\sigma_p)\} \quad \text{Equation 3}$$

Partial differentiation of Eq. (3) at a given deformation temperature yields the n constant. Therefore, the following equations were obtained:

$$n = [\partial \ln \varepsilon^{\circ} / \partial \ln\{\sinh(\alpha\sigma p)\}]_T \quad \text{Equation 4}$$

In next stage, partial differentiation of Eq. (3) at a constant strain rate yields the value of deformation activation energy (Q) according to the following equation:

$$Q = Rn[\partial \ln\{\sinh(\alpha\sigma_p)\} / \partial(1/T)]_{\varepsilon^{\circ}} \quad \text{Equation 5}$$

Based on the literature, the value of constant α is firstly estimated to be 0.012 MPa−1 [1, 5, and 19]. The slope of Ln [Sinh (ασp)] vs Ln εo plot (Figure 4) and Ln [Sinh (α. σp)] vs 10000/T plot (Figure 5) gives the values of A, n and Q, respectively. Therefore, the linear statistical regression analysis of the data results in the average values of $A=2.7\times10^{10}\ s^{-1}$, n=2.6 and Q=263.4 kJ/mol.

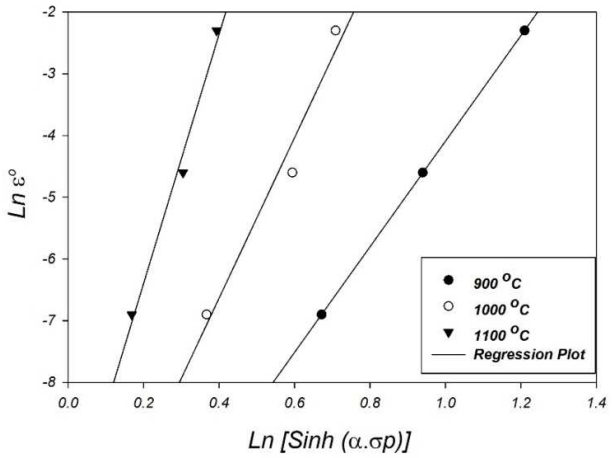

Figure 4: Variations of Peak Stress with Strain Rate for 2205 Duplex Stainless Steel at Different Temperatures

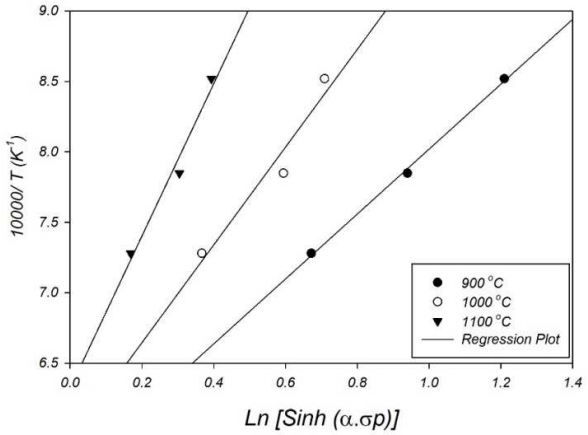

Figure 5: Variations of Peak Stress with Temperature for 2205 Duplex Stainless Steel at Different Strain Rates

According to Eq. [2] and the obtained parameter values, the relationship between Z and σpcan be written as:

$$Z = \dot{\varepsilon} \exp(263 \times 10^3/RT) = 2.7 \times 10^{10} \times [\sinh(0.012 \times \sigma_p)]^{2.6} \quad \text{Equation 6}$$

It is clear that the lower Z values are obtained at higher deformation temperatures; the corresponding Q value is low.

Processing Map

Processing maps are developed on the basis of the principles of dynamic materials model, where the work piece under hot-working conditions is considered as a dissipater of the total power input [7, 19]. The total power (P) consists of two complementary functions G and J:

$$P = \sigma\varepsilon^{o} = G + J = \int_0^{\dot{\varepsilon}^{o}} \sigma \, d\dot{\varepsilon}^{o} + \int_0^{\sigma} \varepsilon^{o} \, d\sigma \quad \text{Equation 7}$$

The quantity G which is given by the area under the true stress - true strain rate curve, is designated as “dissipater power content” and its complementary component J as the “dissipater power co-content”. J in the model is assumed to be related to micro structural changes occurring concomitantly with the deformation, while G is related to continuum effects [3, 20].

In general, most of the dissipation is due to a temperature rise (G content) and a small amount is due to micro structural changes such as DRV, DRX, phase transformations, as well as damage of the material (J co-content).

According to the dynamic constitutive equation ($\sigma = k\dot{\varepsilon}^{m}|_{T,\varepsilon,M}$) for a given applied strain, temperature and initial microstructure, the energy partitioning between G and J is determined by the strain rate sensitivity parameter (m) as follows:

$$\frac{dJ}{dG} = \frac{\dot{\varepsilon} d\sigma}{\sigma d\dot{\varepsilon}} = \frac{\sigma \dot{\varepsilon} dln\sigma}{\sigma \dot{\varepsilon} dln\dot{\varepsilon}} = \frac{\Delta ln\sigma}{\Delta ln\dot{\varepsilon}} = m \quad \text{Equation 8}$$

J and G are formulated as functions of stress, strain rate and m according to the following equation:

$$G = \int_0^{\varepsilon^o} \sigma \, d\varepsilon = \frac{\sigma \varepsilon^o}{1+m} \quad \text{Equation 9}$$

$$J = \int_0^{\sigma} \varepsilon^o \, d\sigma = \frac{m \sigma \varepsilon^o}{1+m} \quad \text{Equation 10}$$

The metallurgical phenomena during deformation may be evaluated by the variation of normalized J co-content with the temperature and strain rate (called efficiency of power dissipation, η). If assume the material is perfectly plastic, work hardening would not occur and m would be maximum, m = 1, and J Max = P/2. Therefore, the efficiency of power dissipation, η, defined by Eq. (11):

$$\eta = J/J_{Max} = 2m/ m+1 \quad \text{Equation 11}$$

On the other hand, the continuum instability criterion for identifying the regimes of flow instabilities, which is based on the maximum rate of entropy, resulted in the following equation:

$$\xi(\dot{\varepsilon}) = \frac{\partial ln\,(m/m+1)}{\partial ln\,\dot{\varepsilon}} + m \; \xi = +m < 0 \text{Equation} \quad \text{Equation 12}$$

Any metallurgical instability manifesting during hot deformation is expected to be revealed in a regime where ξ(ε̇)becomes negative. The processing map is obtained by superimposing the instability map on the power dissipation map.

In the first step, for calculating the strain rate sensitivity factor (m), the experimental data are considered as points and the logarithm of flow stress is plotted against logarithm of strain rate. Then, each curve was fitted with the third order polynomial relationship between log σ and logε̇, m (Figure 6).

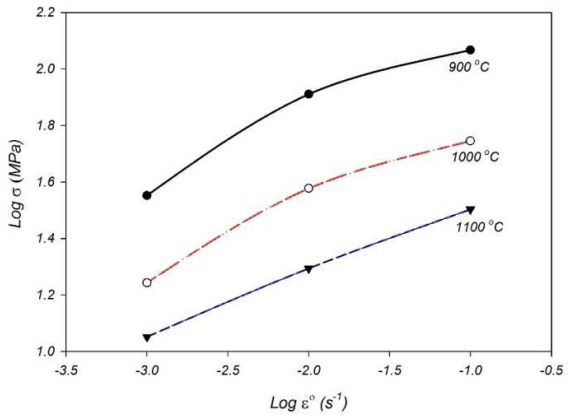

Figure 6: Variation of Log (Flow Stress) With Log (Strain Rate) for Strain of 0.7 to Compute M

The power dissipation map (iso-efficiency contours) and instability map in a two dimensional space obtained at the strain of 0.7 for the cast 2205 duplex stainless steel are exhibited in Figure 7a and b, respectively. It should be noted that the characteristics of the maps at other strains in respect of location of the domains are found to be essentially similar. A superimposition of instability map on power dissipation map as well as related microstructure in different deformation conditions, as shown in Figure 8 gives the processing map which shows the 'unstable' regime on a temperature-strain rate space and should be prevented during actual hot working.

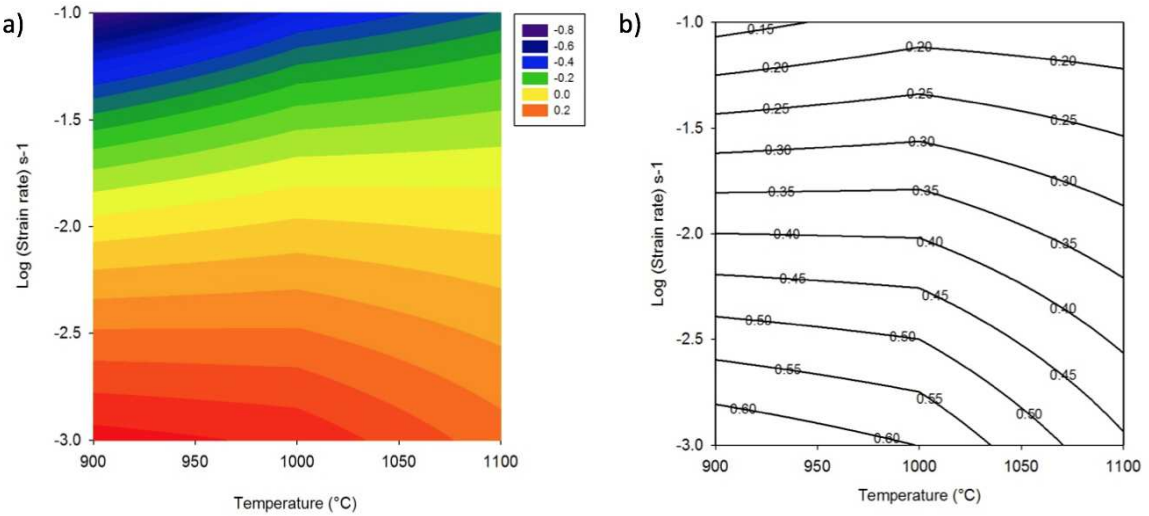

Figure 7: A) Iso-Efficiency Contour of Power Dissipation Map, B) Iso-Efficiency Contour of Instability Map

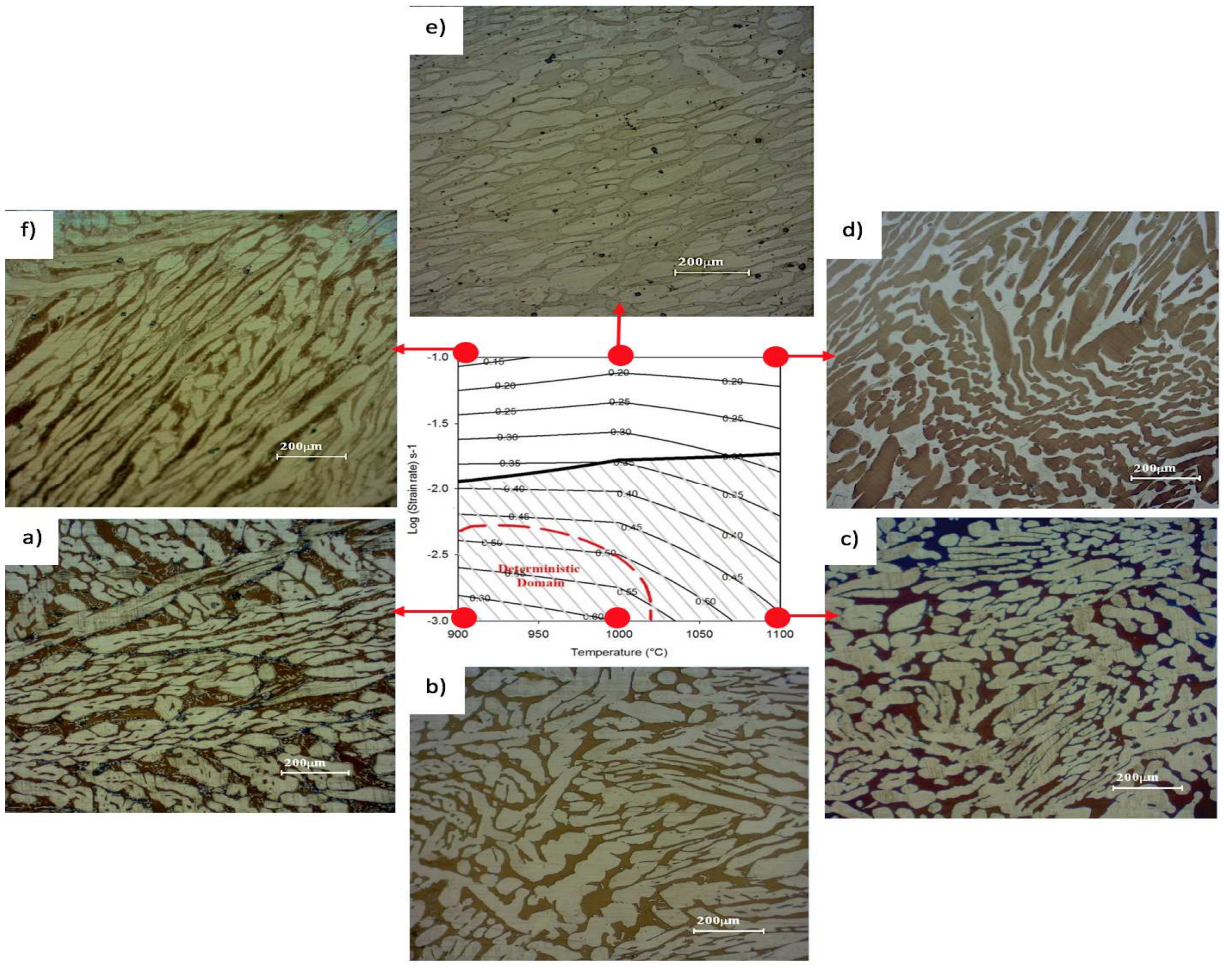

Figure 8: Superimposition of Power Dissipation Map and Instability Map following with the Microstructure under Conditions of a) Strain Rate 0.001 S^{-1} and Temperature 900 ^{o}C, b) Strain Rate 0.001 S^{-1} and Temperature 1000 ^{o}C,c) Strain Rate 0.001 S^{-1} and Temperature 1100 ^{o}C,d) Strain Rate 0. 1 S^{-1} and Temperature 1100 ^{o}C, e) Strain Rate 0. 1 S^{-1} and Temperature 1000 ^{o}C,f) Strain Rate 0. 1 S^{-1} and Temperature 900 ^{o}C,

It should be noted that power dissipation maps are continuum maps and should be interpreted in order to identify 'unsafe' processing condition and to prevent the defect formation such as cracks and cavities, and instability processes. According to Figure 8, one deterministic domain can be determined with peak efficiency values of about 60%. This domain extends over a temperature range of 900-1030 °C and a strain rate range of $\dot{\varepsilon}$ = 0.001-0.003 s^{-1}. The domain is characterized by widely spaced contours typical of a plateau and can be expanded to somewhat lower efficiencies until constrained by the instability regime. Generally, the domain with peak efficiency, in principle, may be interpreted to correspond of DRX [21]. As can be seen from Figure 8a-c, it is clearly apparent that the principle micro structural evolution occurring in the domain is partial and complete DRX of austenite phase. The partial equiaxed austenitic grains distributed within the ferrite matrix, indicating that the DRX of austenitic phases has occurred. It is worth mentioning that, DRX of austenite, which is taken as dominant micro structural changes, is activated by increasing temperature. However, although at higher temperature, efficiency of power dissipation decreases slightly, the state of DRX is similar, as shown in Figure 8b and c.

At the strain rate of about 0.1 s^{-1} in the temperature of 1100 $^{\circ}$C, the microstructures exhibited kinking of austenite and ferrite phase (Figure 8d). It is suggested that the occurrence of kinking under compressive strain is due to buckling, which can be considered to be a type of instability [22].

At high strain rate, decreasing temperature has led to the formation of cavitation, the typical microstructure of which is shown in Figure 8e. It should be related to a mixed microstructure of ferrite and austenite during hot deformation. Thus the cavities may be nucleated continuously at grain boundaries due to high deformation rate and insufficient accommodation of grain boundary sliding [23].

When 2205 duplex stainless steel was hot worked upper 0. 01 s^{-1}, flow localization typical of unstable flow was observed (Figure 8f). As can be seen, deformation has been localized with intense shear banding in particular areas of the microstructure. Generally, at high strain rate deformation conditions, adiabatic heating can lead to highly localized flow along the maximum shear stress plane [24].

CONCLUSIONS

In the present research, the constitutive flow behavior of a 2205 stainless steel has been assessed in the temperature and strain rate ranges of 900-1100°C and 0.001-0.1 s-1, respectively, using the principles of the dynamic material model. A processing, map for hot deformation has been generated indicating different domains and an instability regime illustrating various micro structural mechanisms. In addition, a safe processing window for the defect-free hot deformation of the steel has been identified. The following conclusions can be drawn from this study:

- Optimum hot working domain for a cast 2205 duplex stainless steel can be identified at the temperature range of 900-1030 °C and the strain rate of 0.001-0.003 s-1 which DRX mechanism is activated.
- The 2205 duplex stainless steel is prone to the formation of various micro structural defects during hot working, such as flow localization, kinking and cavities formation.
- The flow stress of 2205 duplex stainless steel during hot deformation is well fitted by the constitutive equation of hyperbolic sine function.
- The average value of activation energy for hot deformation was calculated as 263 kJ mol^{-1}.

REFERENCE

1. Ying Han, DeningZou, Zhiyu Chen, Guangwei Fan, Wei Zhang, Investigation on hot deformation behavior of 00Cr23Ni4N duplex stainless steel under medium–high strain rates, Materials Characterization 62 (2011) 198–203
2. G.W. Fan, J. Liua, P.D. Han, G.J. Qiao, Hot ductility and microstructure in casted 2205 duplex stainless steels, Materials Science and Engineering A 515 (2009) 108–112
3. Y.L. Fang, Z.Y. Liu, H.M. Song, L.Z. Jiang, Hot deformation behavior of a new austenite–ferrite duplex stainless steel containing high content of nitrogen, Materials Science and Engineering A 526 (2009) 128–133
4. M. Faccoli, R. Roberti, Study of hot deformation behaviour of 2205 duplex stainless steel through hot tension tests, Material Science 48 (2013) 5196–5203
5. H. Farnoush, A. Momeni, K. Dehghani, J. Aghazadeh Mohandesi, H. Keshmiri, "Hot deformation characteristics of 2205 duplex stainless steel based on the behavior of constituent phases", Materials and Design 31 (2010) 220–226
6. J.M. Cabrera, A. Mateo, L. Llanes, J.M. Prado, M. Anglada, Hot deformation of duplex stainless steels, Materials Processing Technology 143–144 (2003) 321–325
7. Lei Chen, Xiaocong Ma, Xiao Liu, Longmei Wang, Processing map for hot working characteristics of a wrought 2205 duplex stainless steel, Materials and Design 32 (2011) 1292–1297
8. Shuxia Li, Xueping Ren, Xia Ji, YuanyuanGui, Effects of microstructure changes on the super plasticity of 2205 duplex stainless steel, Materials and Design 55 (2014) 146–151
9. YanyanLiu, HaitaoYan, XinhuaWang, MiYan, Effect of hot deformation mode on the microstructure evolution of lean duplex stainless steel 2101, Materials Science&EngineeringA575(2013)41–47
10. Yinhui Yang, Biao Yan, The microstructure and flow behavior of 2205 duplex stainless steels during high temperature compression deformation, Materials Science and Engineering A 579 (2013) 194–201
11. Ying Han, GuanjunQiao, JiaPeng Sun, DeningZou, A comparative study on constitutive relationship of as-cast 904L austenitic stainless steel during hot deformation based on Arrhenius-type and artificial neural network models, Computational Materials Science 67 (2013) 93–103
12. Prasad, Y.V.R.K., Gegel, H.L., Doraivelu, S.M., Malas, J.C., Morgan, J.T., Lark, K.A. and Barker, D.R., Modeling of dynamic material behavior in hot deformation: forging of Ti-6242, Metallurgical Transactions A, Vol. 15, pp. 1883–1892, 1984.
13. Prasad, Y.V.R.K., Recent Advances in the Science of Mechanical processing, Indian J. Technol., Vol. 28, pp. 435–451, 1990.
14. R. Ebrahimi and A. Najafizadeh, A new method for evaluation of friction in bulk metal forming, J. Mater. Process. Technol., 2004, 152, 136–143.
15. D. Rajabi, A. Abedi, Gh. Ebrahimi, Study on Static Recrystallization Process in Duplex Stainless Steel 2205,

International Journal of ISSI, 8 (2011), 20-23.

16. C.H. Park, J.H. Kim, Y.T. Hyun, J.T. Yeom, N.S. Reddy, The origins of flow softening during high-temperature deformation of a Ti–6Al–4V alloy with a lamellar microstructure, J. Alloys Compd. 582 (2014) 126.
17. Lin YC, Chen Xiao-Min, A critical review of experimental results and constitutive descriptions for metals and alloys in hot working, Materials and Design 32 (2011) 1733–1759
18. R. Ebrahimi, E. Shafiei, Mathematical modeling of single peak dynamic recrystallization flow stress curves in metallic alloys, Shiraz University, chapter 9, 219-224
19. Liu JT, Chang HB, Wu RH, Hsu TY, Ruan XY, Investigation on hot deformation behavior of AISI T1 high-speed steel, Materials Characterization 45 (2000)175–86
20. H.Z. Li, H.J. Wang, X.P. Liang, H.T. Liu, Y. Liu, X.M. Zhang, Hot deformation and processing map of 2519A aluminum alloy, Materials Science and Engineering A 528 (2011) 1548–1552
21. A. Momeni, K. Dehghani, Hot working behavior of 2205 austenite–ferrite duplex stainless steel characterized by constitutive equations and processing maps, Materials Science and Engineering A 528 (2011) 1448–1454
22. T. Seshacharyulu, S.C. Medeiros, W.G. Frazier, Y.V.R.K. Prasad, Micro structural mechanisms during hot working of commercial grade Ti–6Al–4V with lamellar starting structure, Materials Science and Engineering A 325 (2002) 112-125
23. B. Verlinden, J. Driver, I. Samajdar, R. D. Doherty, Thermo mechanical Processing of Metallic Materials, Elsevier, Britain, 2007.
24. S. Tamirisakandala, B.V. Vedam, R.B. Bhat, Recent advances in the deformation processing of titanium alloys, Journal of Materials Engineering and Performance 12 (2003) 661.